Single-camera method to determine the optical axis position of ellipsoidal drops

B. K. Jones, J. R. Saylor, and L. F. Bliven

The sizing of droplets by optical imaging typically requires a small depth of field so that variations in the magnification ratio are minimized. However, if the location of the drop along the optical axis can be determined, a variable magnification ratio can be imposed on each imaged drop, and the depth of field can be increased. Previous research suggested that droplet location can be determined with a characteristic of droplet images that is obtained when the droplet is illuminated from behind. In this prior research, the method was demonstrated with spherical glass objects to simulate raindrops. Raindrops are known to deviate significantly from a spherical shape, especially when the drop size is large. We demonstrate the ability to locate the position of objects that deviate from sphericity. Deformed water drops and glass ellipsoids are tested, along with glass spheres. The role of refractive index is also discussed.

OCIS codes: 120.0120, 010.1100, 280.1100, 000.2170, 110.0110.

1. Introduction

In aerosol and precipitation science, imaging of liquid drops is frequently employed to ascertain droplet size and shape characteristics. To obtain accurate measurements, the magnification ratio must be known and must not vary significantly over the depth of field. Here the magnification ratio is defined as

$$M = \frac{d'}{d}, \tag{1}$$

where d' is the size of the drop in the image and d is the actual drop size.[1] Small f-number optics (small depth of field) are typically used to reduce the variation in magnification ratio for those drops that are imaged. However, it is not always desirable to use small f-number optics. For example, in precipitation science optical measurements are used to obtain statistical characteristics of the size and shape of falling raindrops. In such applications, the number of drops measured per second should be large so that accurate drop statistics can be obtained over short time intervals. This permits observation of details of the storm progression that would not otherwise be apparent. To obtain such a large droplet measurement rate requires a large depth of field, resulting in large errors in measured drop size if a fixed magnification ratio is used. To address this problem, Saylor *et al.*[2] proposed a method to locate the position of an imaged drop along the optical axis using information obtained only from the drop image. This method was experimentally demonstrated with stationary glass spheres to simulate the optical characteristics of raindrops.

In the method of Saylor *et al.*,[2] a camera obtains an image of a drop that is being illuminated from behind. The result is an image having a bright background, a dark drop silhouette, and a bright region in the center of the drop that is an image of the illumination source obtained through the drop. A sample image of a falling water droplet obtained with this configuration is presented in Fig. 1, illustrating these regions. In Saylor *et al.*,[2] the ratio of the size of the light source image (spot size) to the size of the drop image was found to be the important parameter in the determination of the droplet location from a single image. This ratio is defined as

$$\alpha = \frac{d_s'}{d'}, \tag{2}$$

B. K. Jones and J. R. Saylor (jrsaylor@ces.clemson.edu) are with the Department of Mechanical Engineering, Clemson University, Clemson, South Carolina 29634. L. F. Bliven is with the Wallops Flight Facility, NASA Goddard Space Flight Center, Wallops Island, Virginia 23337.

Received 10 May 2002; revised manuscript received 25 October 2002.

0003-6935/03/060972-07$15.00/0

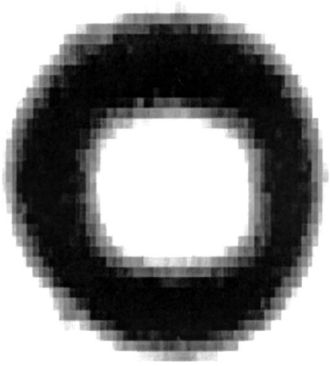

Fig. 1. Sample image of a falling water drop illuminated from behind. The bright spot in the center of the drop is an image of the illumination source, obtained through the drop.

where d_s' is the size of the spot in the image (the image of the light source in the center of the drop) and d' is the size of the drop. Both d' and d_s' are obtained from the image. A monotonic relationship was found between α and the camera-to-drop distance z_d (actually the distance from the camera to the glass sphere in Saylor *et al.*[2]). This relationship, once determined, permits location of the drop along the optical axis when α is computed from the drop image. Once the drop location is known, the correct magnification is implemented to provide an accurate size measurement. It is noted in Saylor *et al.*[2] (and in the present paper as well) that both d_s' and d' are horizontal dimensions.

The primary application of the method described above concerns optical measurement of raindrops. The equilibrium shape of a raindrop is the shape a drop attains as it travels at terminal velocity without oscillations or time-varying behavior. This equilibrium shape is essentially spherical for raindrops that are smaller than approximately 0.3 mm in diameter.[3] Hence the original method attributed to Saylor *et al.*[2] is sufficient for these small drops. However, as the drop size increases, the equilibrium shape deviates significantly from sphericity, becoming an oblate spheroid for intermediate sizes and attaining a flattened base at the largest raindrop sizes.[4] Profiles of the equilibrium shapes of drops ranging from 1 to 6 mm can be found in Beard and Chuang.[5]

At large drop sizes, equilibrium drop shapes are rarely observed because of shape oscillations that distort the drop from its equilibrium shape.[4,6–12] The cause of these oscillations has been attributed to turbulence, aerodynamic forcing such as eddy shedding, as well as droplet collisions.[4] The shapes exhibited by oscillating drops have been observed to be of an essentially ellipsoidal nature[13,14] and have been modeled as a time-varying ellipsoidal variation about an equilibrium shape.[6,7] Our goal in the present study is to ascertain whether the previously obtained relationship between α and z_d can be extended beyond a simple spherical shape to a shape more representative of a raindrop. For this purpose glass ellipsoids were investigated. Actual raindrops do not oscillate about the equilibrium shape in a perfectly ellipsoidal pattern, but instead contain a superposition of spherical harmonics.[3,4] However, for the purposes of the present study, ellipsoidal shapes were deemed sufficient.

Table 1. Dimensions of the Three Ellipsoids Used in This Study

Ellipsoid Number	Major Axis (mm)	Minor Axis (mm)
1	9.04	4.99
2	9.54	6.80
3	10.03	7.78

The successful application of the method described here will permit more accurate measurements of raindrop shapes. Such measurements are useful in the field of remote sensing of rain by use of dual-polarization radars[15–17] in which the drop shape sensitively affects the radar backscatter. These measurements will also be useful in microwave communications applications where signal decorrelation by rain is sensitive to raindrop shape.[18]

2. Experimental Method

The purpose of this study was to ascertain if the method developed by Saylor *et al.*[2] can be extended to nonspherical drops. As described in Section 1, water drops can attain a range of shapes, including ellipsoidal shapes, as they fall. Accordingly, glass ellipsoids were investigated in this study. Several techniques exist that permit the generation of deformed water drops. These include the vibrating orifice aerosol generator,[19] as well as acoustic levitation methods (e.g., Trinh[20]). Glass ellipsoids were used in this study because they could more easily be manipulated and situated within the focal region of the camera.

Three glass ellipsoids were used in this study. The dimensions of the major and minor axes of these ellipsoids are presented in Table 1. We obtained these dimensions by first computing the magnification ratio of the optical setup at a distance of $z_d = 200$ cm. We achieved this by imaging a glass sphere of known diameter at this z_d location. Its diameter in pixels was obtained from the image, and a magnification ratio $M = 18.25$ pixels/mm was computed. We then used this magnification ratio to obtain measurements of the major and minor axes of each ellipsoid by placing that ellipsoid at $z_d = 200$ cm and obtaining its image. Its major and minor axes were measured in pixels from the image and converted to millimeters by use of the known magnification ratio.

The shape of each ellipsoid was quantified by the ratio of the horizontal measure of the ellipsoid a to the vertical measure of the ellipsoid b. For each of the three ellipsoids listed in Table 1, we obtained two values of a/b by conducting experiments with the major axis oriented vertically and with the major axis oriented horizontally, resulting in six values for a/b. Plots of α versus z_d were obtained for each of these a/b values to determine if a/b affected the α versus z_d

Table 2. Values of a/b for Each of the Three Ellipsoids Investigated[a]

Ellipsoid number	a/b, Major Axis Horizontal	a/b, Major Axis Vertical
1	1.82	0.55
2	1.42	0.70
3	1.29	0.78

[a]Two a/b values are given for each ellipsoid. The first value corresponds to a/b with the major axis of the ellipsoid oriented horizontally. The second value corresponds to a/b with the major axis of the ellipsoid oriented vertically.

relationship. The six values of a/b investigated are listed in Table 2.

The values of a/b presented in Table 2 were obtained in the following fashion. Images of each ellipsoid were obtained at approximately 40–80 locations within the range of z_d investigated in the experiments. At each of these locations a and b were measured for each ellipsoid. The value of a/b was computed for each location and then averaged over all the locations at which images were obtained. These values are presented in Table 2 for each ellipsoid in each of its two orientations. This procedure of computing a/b from many images obtained over a range of z_d reduced pixelization errors. A consequence of this is that the a/b values listed in Table 2 deviate slightly from those that would be obtained with the data in Table 1 because the Table 1 data were obtained from a single image at a single z_d location.

The setup used to obtain images is presented in Fig. 2, which actually describes the setup used for the glass spheres and ellipsoids. A slight modification was necessary to image falling water drops, as we describe below. The components of the experimental apparatus consisted of a rectangular halogen lamp and a CCD video camera (monochrome mini-CCD camera, Model PC28C, Supercircuits Inc., Liberty Hill, Tex.) fitted with a 220-mm lens. A diffuser was placed in front of the lamp, which consisted of a frosted glass plate and a layer of frosted plastic filter paper (Lee Filters USA, Burbank, Calif., filter numbers 129). The object being imaged (drop, sphere, or ellipsoid) was located on the optical axis, in between the lamp and the camera, at a distance z_d from the front of the camera lens. The value of z_d was varied over a range of ~100 cm, typically in 1-cm intervals. The camera-to-lamp distance z_l was fixed at a value of

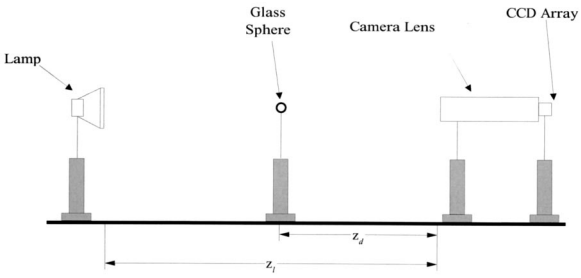

Fig. 2. Experimental setup used to investigate glass spheres and ellipsoids.

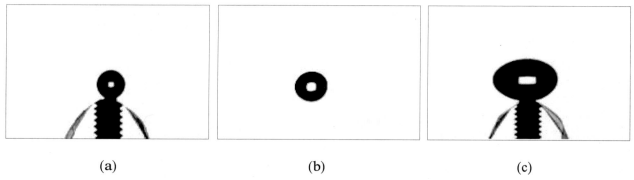

Fig. 3. Sample images of (a) glass sphere, (b) falling water drop, (c) glass ellipsoid. The horizontal dimension of these three are 4.0, 4.2, and 10 mm, respectively. The glass objects presented in images (a) and (c) are supported on a small set screw that can be seen protruding from the bottom of the image. Also visible in (a) and (c) is a curved piece of double-sided tape that was used to attach the glass to the set screw.

260 cm for all experiments. Sample images obtained with this setup are presented in Fig. 3 for a glass sphere, a falling water drop, and a glass ellipsoid. A PC with data-acquisition and image processing software was used to acquire, store, and process the images.

The goal of this study was to obtain plots of α versus z_d for ellipsoids and deformed water drops and to determine if the α versus z_d behavior obtained is the same as that obtained for spherical objects. For each object tested, images were obtained over a range of z_d, and values of α were computed at each z_d. The results were compiled in the form of α versus z_d plots.

As defined in Eq. (2), α is the ratio of d_s' to d'. In the present study, d_s' and d' both refer to a horizontal measurement. Hence d_s' is the width of the spot seen in the center of the ellipsoid image, and d' is the width of the ellipsoid outline. This choice is arbitrary, and a vertical dimension could have been used. This would have resulted in smaller values for α because the shape of the lamp is rectangular, with the longer dimension horizontal. Hence d_s' would be smaller in the vertical dimension. This would have simply resulted in a vertical shift in the α versus z_d plots. Here we use horizontal measurements to maintain continuity with our prior study (Saylor *et al.*[2]).

We measured the α ratio using image processing tools in IMAQ, a module of the LabVIEW environment. The following steps were used to obtain α. First we converted the 8-bit image obtained by the video camera to a binary image using a threshold. The threshold was obtained by use of the clustering algorithm in the IMAQ thresholding menu. This algorithm divides the image histogram into two classes, and the threshold is obtained from the average of the centroid intensity for the two classes. We created a binary image by setting all pixels greater than the threshold to 1 and all pixels less than the threshold to 0. After we transformed the image into a binary format, the width of the drop outline and the width of the spot were obtained, and we computed α using Eq. (2).

Images of glass spheres and ellipsoids were obtained with the apparatus presented in Fig. 2 where the glass object was supported on a vertical pedestal. A slight modification to this apparatus was necessary to obtain images of falling water drops. This modi-

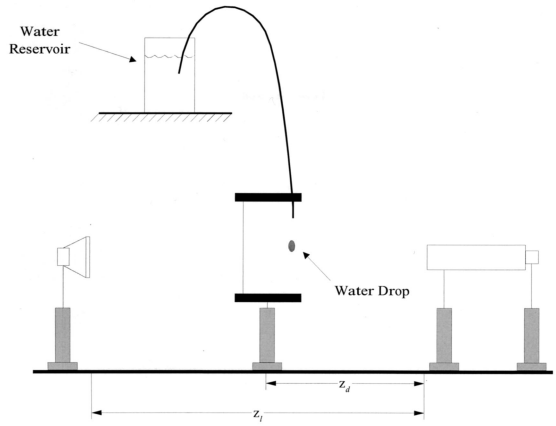

Fig. 4. Experimental setup used to image falling water drops.

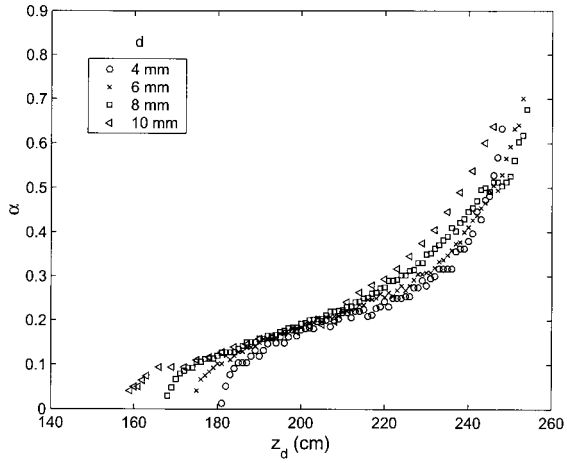

Fig. 5. Plot of α versus z_d for glass spheres of diameter d = 4, 6, 8, and 10 mm.

fied apparatus is illustrated in Fig. 4. We obtained images of falling water drops by replacing the vertical post with a dropper apparatus that was positioned at discrete locations along the optical rail. Drops were formed at the tip of a length of 0.05-in.-(0.13-cm) i.d. Tygon tubing that was connected to a water reservoir. The drops were allowed to fall from the outlet of the tube, located 35 cm above the measurement volume, and images were obtained as the drops fell through the measurement volume. Measurements of α were obtained with the same image processing algorithm described above.

Blurring occurred when the same CCD integration time used for the stationary glass objects was used for the falling water drops. To eliminate blurring, the CCD integration time was reduced and the light intensity was increased when the 150-W bulb in the lamp was replaced with a 500-W bulb. Drop images obtained under these conditions were not blurred. At this larger illumination intensity and shorter integration time, the pixel intensities obtained from an image of a fixed object were different from those obtained with the original integration time and light intensity. This affected the pixel histogram, which in turn affected the thresholding value computed during drop image processing and concomitantly affected the value of d_s' obtained from the image. To alleviate this problem, it was necessary to ensure that the image intensities were identical for the two lighting conditions used. To do this, the black-and-white reference voltages of the CCD array were manually altered for the large illumination case. These reference voltages determine the light intensities corresponding to pure white and pure black in the output image. These voltages were adjusted so that d_s' obtained from a test image of an 8-mm glass sphere was the same for the 500-W bulb and 150-W bulb cases. The adjusted voltages were then used during acquisition of the falling drop images. It should be noted that this procedure of forcing d_s' to be equal was conducted at a single value of z_d. Hence this procedure did not force the α versus z_d behavior of two different objects to be the same. It should also be noted that, in a field application, a single light intensity and integration time would be employed, and that calibration plots of α versus z_d would have to be conducted to implement this method.

3. Results

The α versus z_d plots for glass spheres, glass ellipsoids, and water drops are now presented. In Fig. 5, plots of α versus z_d for four glass spheres of diameter d = 4, 6, 8, and 10 mm are presented. These plots are essentially a reproduction of the research presented in Saylor *et al.*[2] The close proximity of each plot indicates that the α versus z_d behavior is not a function of diameter for spherical objects. The range of z_d presented in Fig. 5 (as well as for the other α versus z_d plots to follow) is dictated by the range over which a spot is observed in the image of the glass sphere (or glass ellipsoid or water drop, as the case may be). At large z_d, the spot in the image approaches the size of the object outline, and α cannot be computed. For small z_d, the spot approaches the size of one or two pixels, and α cannot be accurately computed. The range of z_d in between these two limiting values is the range over which data are included in the α versus z_d plots presented here. It is noted that the range of z_d over which a spot is observed is also the range of z_d for which the object appears in focus and therefore is an excellent method for rejection of out-of-focus drops in field implementations of this method.

In Fig. 6, plots of α versus z_d are presented for glass ellipsoids of varying axis ratios. Axis ratio is defined as a/b, where a is the horizontal axis of the ellipsoid and b is the vertical axis. As noted in Section 2, we obtained these data by imaging three glass ellipsoids, each in its horizontal and vertical orientation. Plots of α versus z_d for five values of a/b are presented. A sixth data set, corresponding to an ellipsoid with a/b = 1.82, was also obtained (and is listed in Table 2) but was omitted because of aberrations in the shape of the glass ellipsoid when it was oriented to give a/b = 1.82. It is noted that, for actual raindrops, maximum values of a/b differ from 1.0 by only

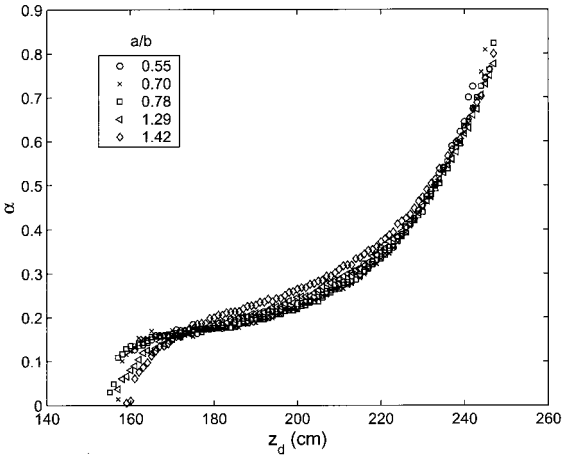

Fig. 6. Plot of α versus z_d for glass ellipsoids with $a/b = 0.55, 0.70, 0.78, 1.29, 1.42$.

~40%, and a value of 1.82 would be highly unusual.[11,12,17] Hence eliminating this data set does not significantly affect application of these results to raindrops. The data sets presented in Fig. 6 closely agree with each other, indicating that variations in a/b do not change α versus z_d behavior.

In Fig. 7, the data from Figs. 5 and 6 are combined to provide a plot of α versus z_d for glass spheres and ellipsoids. Taken as a group, the data exhibit a vertical scatter of approximately 10%. However, looking at the glass sphere and glass ellipsoid data separately, it can be seen that the glass sphere data are slightly displaced in the vertical direction from the ellipsoidal data. As will be demonstrated in Section 4, this displacement does not affect the utility of the method because it is due to index of refraction effects.

The final data set obtained was for falling water drops. A plot of α versus z_d for ~4 mm water drops

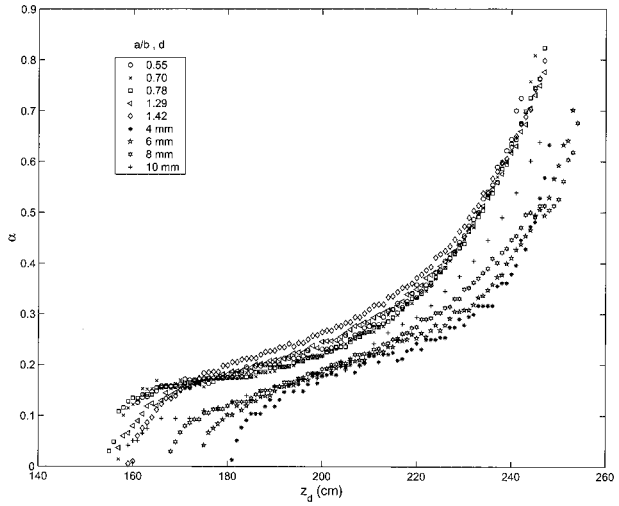

Fig. 7. Plot of α versus z_d for glass spheres and glass ellipsoids. The numbers listed in the legend correspond to the diameter in millimeters for the glass spheres and the value of a/b for the glass ellipsoids.

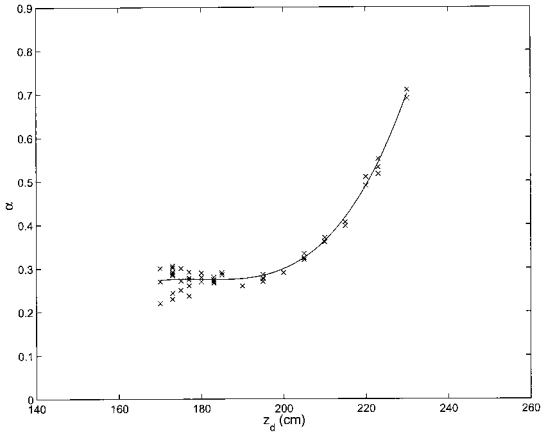

Fig. 8. Plot of α versus z_d for falling water drops. $d \sim 4$ mm.

is shown in Fig. 8. The α versus z_d data obtained for these water drops are well fit by a cubic:

$$\alpha = a_3 z_d^{\,3} + a_2 z_d^{\,2} + a_1 z_d + a_0\,, \qquad (3)$$

where $a_3 = 3.5305 \times 10^{-6}$, $a_2 = -0.0019094$, $a_1 = 0.34406$, $a_0 = -20.381$, and z_d is in centimeters. This curve fit is included in Fig. 8. It should be noted that, in contrast to the data for glass ellipsoids, a/b is not controlled for the water-drop experiments. The range of a/b for the data presented in Fig. 8 simply corresponds to the range in a/b that the measured drops displayed as they fell through the measurement volume.

The data presented in Fig. 8 can be used as an example revealing the depth of field over which drops can be imaged without inaccuracies in sizing. The data presented in Fig. 8 were obtained over a range of z_d from 170 to 230 cm. Hence the depth of field over which drops were imaged is 60 cm for the optical setup used here. Equation (3) was obtained from these data. Using this same setup, Eq. (3) can be used to ascertain z_d in subsequent drop images when we compute α from the image. Once α is known, the appropriate magnification ratio can be obtained, and an accurate measure of the drop can be obtained over the entire 60-cm depth of field.

The data for water are replotted with the data for a glass sphere and a glass ellipsoid in Fig. 9. The shape of all three curves is the same; however, all three data sets are vertically displaced from each other, with the uppermost plot being for the water drops, the middle data set for the glass ellipsoid, and the lowest data set for the glass sphere. The reason for the separation of these data sets, as well as for the 10% scatter in Fig. 7, is addressed in Section 4.

4. Discussion

The ultimate goal of the research presented here is to develop a method that locates the position of a raindrop along the optical axis of a single camera. Following the study of Saylor *et al.*[2], the variable α was used to correlate the location of the drop along the optical axis of the camera. This prior study demon-

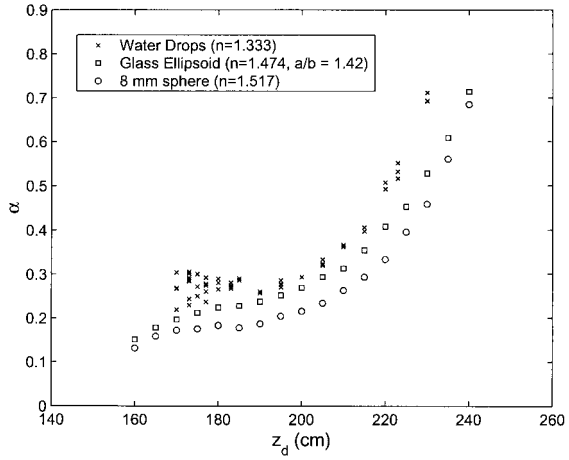

Fig. 9. Plot of α versus z_d for falling water drops, a glass ellipsoid, and a glass sphere. For the glass sphere the diameter is 8 mm, and for the glass ellipsoid the value of a/b is 1.42.

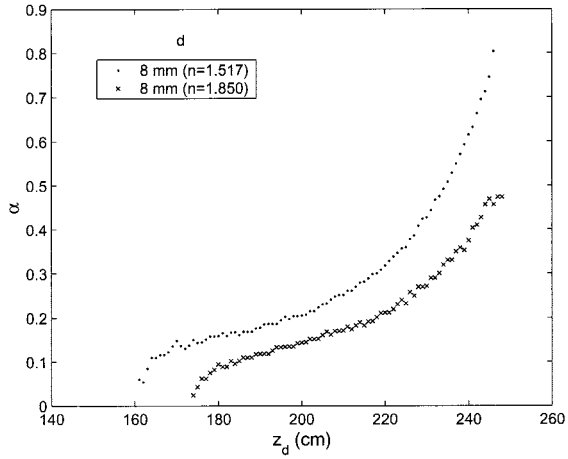

Fig. 10. Plot of α versus z_d for two 8-mm spheres with different indices of refraction.

strated a one-to-one correlation between α and z_d. A concern was that this relation would not hold for objects of ellipsoidal shape, e.g., ellipsoidally deformed drops. Specifically, the possibility that the α versus z_d relationship would change with a/b was a concern. Figure 6 reveals that this is not the case. For a/b ranging from 0.55 to 1.42, and for z_d ranging from 170 to 240 cm, the α versus z_d relationship is essentially independent of a/b. This plot suggests that use of an α versus z_d relationship to locate the position of a falling raindrop along the optical axis of a camera should work well whether the drop being imaged is spherical or ellipsoidally deformed. It should be noted that the values of α obtained at a given z_d will change with illumination intensity, exposure time, and ambient light level. Hence implementation of this method in the field requires one to obtain calibration plots of α versus z_d for the specific optical setup used.

A sphere is simply an ellipsoid with $a/b = 1$. Hence the results of Fig. 6 suggest that good agreement should exist between the glass ellipsoid and the glass sphere data sets. However, when the data for glass ellipsoids and glass spheres are plotted on the same axis in Fig. 7, the agreement between the two sets shows a variation of approximately 10%. It is clear (particularly at large z_d) that the data for spheres and ellipsoids fall into two distinct groups. Although this seems to suggest that spheres and ellipsoids have different α versus z_d behavior, careful examination of Fig. 7 suggests that this is not the case. The ellipsoidal data presented in Fig. 7 do not get closer to the spherical data as $a/b \rightarrow 1$, which one would expect because $a/b = 1$ defines a sphere. Hence a different explanation must be sought.

It was noted that the index of refraction of the glass used to make the spheres and ellipsoids differed. The index of refraction was $n = 1.474$ for the ellipsoids and $n = 1.517$ for the spheres. We hypothesized that the displacement between the glass spheres and the glass ellipsoids was due to this index of refraction effect. To test this hypothesis, we obtained α versus z_d plots of two glass spheres of identical diameter, but with a different index of refraction. These data are plotted in Fig. 10 for two 8-mm-diameter spheres having $n = 1.517$ and $n = 1.850$. A significant vertical offset between these two plots is displayed, with the lower index of refraction plot located above the higher index of refraction plot. In Fig. 7, the ellipsoidal data are located above the sphere data, and the ellipsoid has a lower index of refraction than the sphere, suggesting that this offset is due to index of refraction differences and is not due to the geometry of the two objects. Hence the reasonable agreement between the glass sphere and the ellipsoid data presented in Fig. 7 would be even better had the two sets of objects been made from the same type of glass.

The index of refraction effect described above also explains the large vertical offset between the water drop, the glass ellipsoid, and the glass sphere data plotted in Fig. 9. In this plot, water drops having the lowest index of refraction, $n = 1.333$, are located above the ellipsoids having $n = 1.474$; the glass spheres having the largest index of refraction, $n = 1.517$ are shown in the lowest plot, agreeing with the trend displayed in Fig. 10. Hence, although the three data sets plotted in Fig. 9 show significant vertical displacement, the relevant point to take note of is the similarity in the shape of these curves. This similarity suggests that the water drops can be located along the optical axis when we use an equation having the same form as Eq. (3), regardless of the shape that the drop might attain.

Water displays a variation in index of refraction with temperature that might result in errors. However, over a range from 15 °C to 34 °C, n varies from 1.33341 to 1.33136 for water.[21] This 0.2% variation is small compared with the 70% variation in n for the glass used in the spheres and ellipsoids. Hence temperature variations should not limit the ability of this method to locate a drop on the optical axis.

We computed the values of α presented here by

dividing the internal spot width by the outer drop width. For small drops, these diameters can be represented by a small number of pixels, adding noise to the measurement. In future implementations, the areas of the spot and the entire drop will be used to compute α. When an area measurement is used, a larger number of pixels is incorporated, resulting in less scatter in the data when the drop size is small.

Finally, some discussion is needed regarding the divergence in the data for the water drops seen at the low z_d end of the data plotted in Fig. 8, where the falling drops are being randomly imaged. The shape in each image is whatever shape the drop happens to have at the moment when image acquisition occurs. Hence the a/b values vary for each of the several images obtained at each z_d. We have shown that α is independent of a/b. However, as Fig. 6 shows, this a/b independence fails for small z_d. In Fig. 6, each a/b plot separates at small z_d. Hence in Fig. 8, as a/b varies from image to image, α varies, explaining the variation in the data seen in Fig. 8. This variation is not significant regarding the overall goals of this study. It simply defines the range of applicability of the α versus z_d relationship.

5. Conclusion

A correlation between the position of a water drop on the optical axis of a camera is developed. This correlation is a function of one variable, α, which is the ratio of the width of the inner bright spot in the drop to the width of the drop outline in the drop image. Because α can be computed from a single image, the drop location can be determined with only one camera, thereby avoiding complicated stereographic imaging methodologies. This method permits increases in the depth of field of the camera, without sacrificing the accuracy of the drop size measurement. For the particular setup used here, water-drop images were acquired over a depth of field of 60 cm without sacrificing measurement accuracy.

Primary funding for this project came from NASA, whose support is gratefully acknowledged. J. R. Saylor was supported by NASA through the South Carolina Space Grant Consortium. L. F. Bliven was funded by NASA Headquarters under RTOP 622-47-12. B. K. Jones was partially supported by the National Science Foundation Research Experiences for Undergraduates Program.

References

1. F. A. Jenkins and H. A. White, *Fundamentals of Optics* (McGraw-Hill, New York, 1957).
2. J. R. Saylor, B. K. Jones, and L. F. Bliven, "A method for increasing depth of field during droplet imaging," Rev. Sci. Instrum. **73,** 2422–2427 (2002).
3. T. Nousiainen and K. Muinonen, "Light scattering by Gaussian, randomly oscillating raindrops," J. Quant. Spectrosc. Radiat. Transfer **63,** 643–666 (1999).
4. K. V. Beard, H. T. Ochs, and R. J. Kubesh, "Natural oscillations of small raindrops," Nature (London) **342,** 408–410 (1989).
5. K. V. Beard and C. Chuang, "A new model for the equilibrium shape of raindrops," J. Atmos. Sci. **44,** 1509–1524 (1987).
6. K. V. Beard, "Raindrop oscillations: evaluation of a potential flow model with gravity," J. Atmos. Sci. **41,** 1765–1774 (1984).
7. K. V. Beard, "Oscillation models for predicting raindrop axis and backscatter ratios," Radio Sci. **19,** 67–74 (1984).
8. K. V. Beard and R. J. Kubesh, "Laboratory measurements of small raindrop distortion. Part 2: Oscillation frequencies and modes," J. Atmos. Sci. **48,** 2245–2264 (1991).
9. K. V. Beard and A. Tokay, "A field study of raindrop oscillations: observations of size spectra and evaluation of oscillation causes," Geophys. Res. Lett. **18,** 2257–2260 (1991).
10. R. J. Kubesh and K. V. Beard, "Laboratory measurements of spontaneous oscillations for moderate-size raindrops," J. Atmos. Sci. **50,** 1089–1098 (1993).
11. A. Tokay and K. V. Beard, "A field study of raindrop oscillations. Part 1: Observation of size spectra and evaluation of oscillation modes," J. Appl. Meteorol. **35,** 1671–1687 (1996).
12. K. Andsager, K. V. Beard, and N. F. Laird, "Laboratory measurements of axis ratios for large raindrops," J. Atmos. Sci. **56,** 2673–2683 (1999).
13. D. C. Blanchard, "The behavior of water drops at terminal velocity in air," Eos Trans. Am. Geophys. Union **31,** 836–842 (1950).
14. D. M. A. Jones, "The shape of raindrops," J. Meteorol. **16,** 504–510 (1959).
15. G. C. McCormick, A. Hendry, and B. L. Barge, "The anisotropy of precipitation media," Nature (London) **238,** 214–216 (1972).
16. T. A. Seligia and V. N. Bringi, "Potential use of radar differential reflectivity measurements at orthogonal polarizations for measuring precipitation," J. Appl. Meteorol. **5,** 69–76 (1976).
17. C. W. Ulbrich, "A review of the differential reflectivity technique of measuring rainfall," IEEE Trans. Geosci. Remote Sens. **GE-24,** 955–965 (1986).
18. T. Oguchi, "Scattering from hydrometeors: a survey," Radio Sci. **16,** 691–730 (1981).
19. R. N. Berglund and R. Y. H. Liu, "Generation of monodisperse aerosol standards," Environ. Sci. Technol. **7,** 147–153 (1973).
20. E. H. Trinh, "Compact acoustic levitation device for studies in fluid dynamics and material science in the laboratory and microgravity," Rev. Sci. Instrum. **56,** 2059–2065 (1985).
21. R. C. Weast, *Handbook of Chemistry and Physics*, 52nd ed., (Chemical Rubber Co., Cleveland, Ohio, 1972).